Dynamics of acoustically levitated disk samples

W. J. Xie* and B. Wei
Department of Applied Physics, Northwestern Polytechnical University, Xi'an 710072, People's Republic of China
(Received 18 February 2004; revised manuscript received 2 June 2004; published 28 October 2004)

The acoustic levitation force on disk samples and the dynamics of large water drops in a planar standing wave are studied by solving the acoustic scattering problem through incorporating the boundary element method. The dependence of levitation force amplitude on the equivalent radius R of disks deviates seriously from the R^3 law predicted by King's theory, and a larger force can be obtained for thin disks. When the disk aspect ratio γ is larger than a critical value $\gamma^*(\approx 1.9)$ and the disk radius a is smaller than the critical value $a^*(\gamma)$, the levitation force per unit volume of the sample will increase with the enlargement of the disk. The acoustic levitation force on thin-disk samples ($\gamma \leqslant \gamma^*$) can be formulated by the shape factor $f(\gamma, a)$ when $a \leqslant a^*(\gamma)$. It is found experimentally that a necessary condition of the acoustic field for stable levitation of a large water drop is to adjust the reflector-emitter interval H slightly above the resonant interval H_n. The simulation shows that the drop is flattened and the central parts of its top and bottom surface become concave with the increase of sound pressure level, which agrees with the experimental observation. The main frequencies of the shape oscillation under different sound pressures are slightly larger than the Rayleigh frequency because of the large shape deformation. The simulated translational frequencies of the vertical vibration under normal gravity condition agree with the theoretical analysis.

DOI: 10.1103/PhysRevE.70.046611 PACS number(s): 43.25.+y

I. INTRODUCTION

An intense acoustic field can exert a substantial force on the object immersed in it. This is known as the acoustic radiation force and can be applied to levitate substances for containerless processing [1–3]. In the last few decades, acoustic levitation has found a variety of application fields, such as solidification [4–6], fluid dynamics [7,8], and even biology [9,10]. Since King's pioneering work [11], the acoustic radiation force is generally evaluated on samples with a spherical shape [12,13]. In an incident plane standing wave, $\Phi_{in}=\Phi_0 \sin(kz)e^{-j\omega t}$, where Φ_0 is the amplitude of the velocity potential, $k=2\pi/\lambda$ is the wave number, and $\omega=2\pi f$ is the angular frequency, the acoustic radiation force on a small rigid sphere can be expressed as [11]

$$F = -\tfrac{5}{6}\pi\rho_0\Phi_0^2(kR_S)^3\sin(2kz), \tag{1}$$

where ρ_0 is the density of the medium, R_S is the radius of the sphere, and z is the position where the sphere is located. The minus sign appears in Eq. (1) because the origin $z=0$ is chosen at the pressure node rather than the antinode.

Theoretically, Eq. (1) is only valid when the sample is spherical and its radius $R_S \ll \lambda$. For spheres that have a finite radius, Eq. (1) has to be modified as [14]

$$F = F_0 f(R_S), \tag{2}$$

in which F_0 is the value of the force at the limit $kR_S \to 0$, and f is the shape factor derived by Leung *et al.* [14],

$$f(R_S) = \frac{3}{(2kR_S)^2}\left(\frac{\sin(2kR_S)}{2kR_S} - \cos(2kR_S)\right). \tag{3}$$

In the limit $kR_S \to 0$, Eq. (2) is actually reduced into Eq. (1).

In fact, nonspherical samples are frequently levitated and studied in experiments [2,4,15]. For example, liquid drops levitated in a single axis-acoustic levitator often take a disklike shape and this shape is usually preserved after solidification. In the experiment of containerless melting and solidification of metallic materials, the solid samples are also preshaped into a disk to avoid violent instability aroused by the large shape deformation during the melting process [4]. Therefore, it is necessary to evaluate the acoustic levitation force on disklike samples in order to have a better control of the acoustic levitation processing. On the other hand, the levitation force seems to increase when a sphere is compressed into a disk [15]. But a quantitative knowledge of this phenomenon is still lacking. This paper presents a numerical study of the acoustic levitation forces on disk samples in a standing wave. The dependence of the levitation force on the disk size and shape will be discussed.

The kinematics and dynamics of a levitated drop in acoustic field is of interest in the areas of fluid dynamics and containerless solidification, and have attracted extensive research both theoretically and experimentally [16–26]. This is also the physical basis to measure the surface tension and viscosity of liquids by the acoustic levitation method [27–29]. A drop levitated in an acoustic field experiences nonuniform acoustic radiation force on its surface, and deforms from its original spherical shape. The interaction on the drop by acoustic radiation pressure, surface tension, and gravity generally produces translational vibration, shape oscillation, and rotation.

Marston *et al.* [16] and Jackson [17] studied the small deformation of acoustically levitated drops and formulated

*Corresponding author. Email address: lmss@nwpu.edu.cn

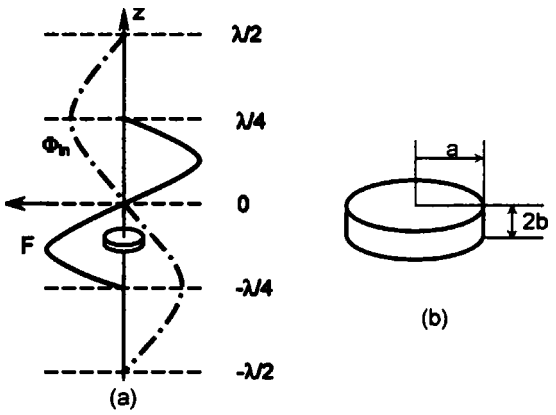

FIG. 1. Schematic of a disk levitated in a plane standing sound wave. (a) Geometry of the scattering problem. The dot-dashed line represents the incident velocity potential distribution and the solid line represents the acoustic radiation force. The arrows represent the positive direction of the force F. (b) Definition of the disk parameters. The disk shape is characterized by its aspect ratio $\gamma=a/b$.

the equilibrium shape that is slightly off a sphere. The oscillation frequency of a spherical drop in free space can be described by the classical Rayleigh relationship [27]. The numerical method developed by Shi *et al.* [18] and Su *et al.* [19] was able to simulate a large deformation and also to obtain the oscillational frequencies of nonspherical drops. The oscillation frequency was found to vary with the drop deformation, and corresponding investigations have been attempted by Trinh *et al.* [20], Suryanarayana *et al.* [21], Zheng *et al.* [22], and Shi *et al.* [23], either experimentally or numerically. But their conclusions are not in good agreement with each other. The disintegration of levitated drop by atomization often results in the failure of experiments [24]. Danilov *et al.* [25] proposed the critical condition of atomization, which was further identified by Anilkumar [26].

This paper also presents an experimental investigation and numerical simulation of the deformation and oscillation of acoustically levitated water drops. The condition of acoustic field for stable levitation of drops is analyzed. Based on the dynamic evolution of water drops under different conditions, the equilibrium shape, translational frequency, and oscillational frequency are determined and discussed with respect to sound pressure.

II. ACOUSTIC LEVITATION FORCE ON RIGID DISK SAMPLES

A. Model of acoustic levitation for disk samples

Figure 1 shows the schematic of a rigid disk sample with radius a and thickness $2b$ inside a time-harmonic standing wave field. The shape of the disk is characterized by the ratio of its diameter to thickness, $\gamma=a/b$. The larger the γ value, the thinner the disk shape is. When $\gamma=1.0$, the thickness of the disk is identical to its diameter, which corresponds to a very "thick" disk. In the following studies, only disks with $\gamma\geqslant 1$ will be considered. The symmetric axis of the disk is parallel to the traveling direction of an acoustic wave. This is an acoustic scattering problem. The resultant velocity potential is the sum of the incident term and the scattering term, $\Phi=\Phi_{\text{in}}+\Phi_{\text{sc}}$, and the spatial part of Φ satisfies the Helmholtz equation,

$$\nabla^2\Phi + k^2\Phi = 0 \tag{4}$$

with the boundary condition $\partial\Phi/\partial n=0$ on the disk surface. Equation (4) can be further transformed into the boundary integral equation over the surface of the disk, and then solved by the boundary element method,

$$C(\mathbf{r})\Phi(\mathbf{r}) = \Phi_{\text{in}}(\mathbf{r}) + \int\int \Phi(\mathbf{r}')\frac{\partial}{\partial n'}G(\mathbf{r},\mathbf{r}')dS'. \tag{5}$$

Here, $G(\mathbf{r},\mathbf{r}')=(4\pi|\mathbf{r}-\mathbf{r}'|)^{-1}\exp(jk|\mathbf{r}-\mathbf{r}'|)$ is the free-space Green function. $C(\mathbf{r})$ is a constant related to the geometric characteristics at the point $\mathbf{r}$ and the value of $4\pi C$ is equal to the solid angle enclosed by the sample surface at $\mathbf{r}$.

The acoustic radiation pressure is the average effect of the vibrating medium on the sample surface during a period of time. King's theory gives the relationship between the time-averaged radiation pressure P and the velocity potential Φ on the sample surface [11],

$$P = \left\langle \frac{1}{2}\rho_0 k^2\Phi^2 - \frac{1}{2}\rho_0(\mathbf{t}\cdot\nabla\Phi)^2 \right\rangle, \tag{6}$$

where $\mathbf{t}$ is the unit tangential vector along the sample surface, and $\langle\rangle$ denotes the time average over a period of acoustic wave.

The total acoustic radiation force exerted on the sample can be calculated by integrating the z component of this radiation pressure over the sample surface,

$$F = -\int\int P\cos(\mathbf{n}\wedge\mathbf{z})dS. \tag{7}$$

For simplicity and generalization of the following calculation, all of the above equations are transformed into dimensionless forms. The characteristic length, potential, and density are chosen as λ, Φ_0, and ρ_0, respectively. In this way, the incident velocity potential will be $\Phi_{\text{in}}=\sin(2\pi z)$. King's formula of acoustic radiation force [Eq. (1)] and radiation pressure [Eq. (6)] becomes $F=-\frac{5}{6}\pi(2\pi R_S)^3\sin(4\pi z)$ and $P=\langle 2\pi^2\Phi^2-(\mathbf{t}\cdot\nabla\Phi)^2/2\rangle$, respectively.

For a spherical sample, Eq. (2) shows that the acoustic radiation force has a sinusoidal distribution along the z direction with a spatial period of $\lambda/2$, and the force amplitude is dependent on the sphere radius by $\sim R_S^3 f(R_S)$. Since the disk sample is symmetric about its middle plane, it is expected that the corresponding force is also a sinusoidal function of z similar to Eq. (2). Therefore, it is only necessary to study the variation of the levitation position between $-\lambda/4$ and $\lambda/4$, and to reveal the relationship between the maximum force (obtained at $z=-\lambda/8$) and the disk parameters (γ and a). In order to make a comparison between the disks and spheres, the equivalent radius of the disk, R, is defined as the radius of a sphere that occupies the same volume of this disk, and the concept of shape factor $f(a,\gamma)$ for disks is also applied. The acoustic radiation pressure has an oscillatory distribution over the sample surface because of the oscillatory

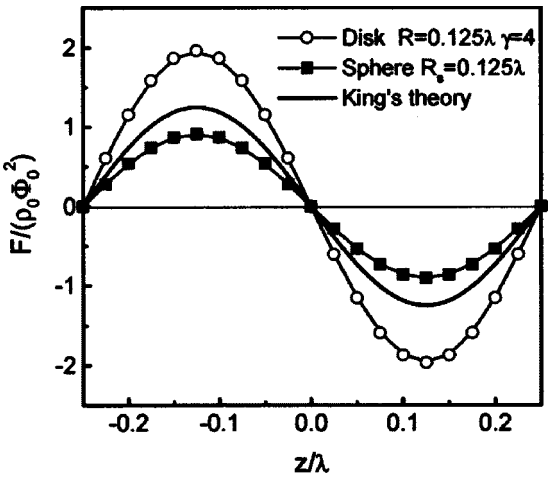

FIG. 2. Variation of the acoustic radiation force F on a sphere and a disk when the sample moves from $-\lambda/4$ to $\lambda/4$ along the z direction. The radius of the sphere and the equivalent radius of the disk are both equal to 0.125λ.

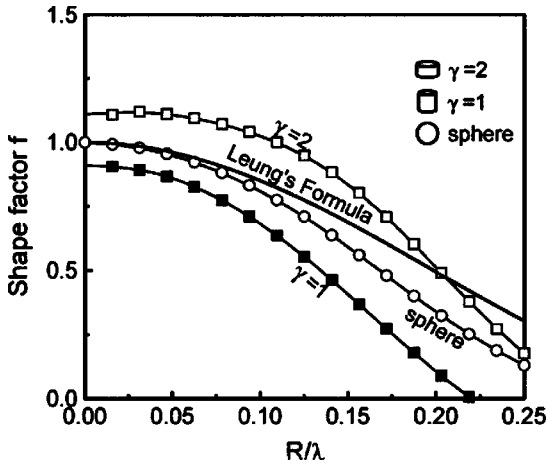

FIG. 3. Dependence of the shape factor f on sphere radius. The simulated data (open circles) show good agreement with Leung's theory when $R\rightarrow 0$ but significantly deviate from that when $R\rightarrow\lambda/4$. The data for disks with $\gamma=1$ (solid squares) and $\gamma=2$ (open squares) are also plotted as a reference.

characteristics of the incident acoustic field. If the geometry of the sample reaches $\lambda/2$ (the spatial period of acoustic radiation force), the oscillatory pressure variation over the sample surface will counteract each other and only a small levitation force can be obtained. Therefore, the equivalent radius of the disk will be confined to $R\leqslant\lambda/4$ in the following calculation to meet the needs of actual applications.

B. Dependence of acoustic levitation force on disk size and shape

Figure 2 shows the variation of the acoustic radiation force on a sphere and a disk when the sphere or disk moves from $-\lambda/4$ to $\lambda/4$ along the z axis. The disk has a shape characteristic of $\gamma=4$ and its equivalent radius R is equal to the radius of the sphere: $R=R_S=0.125\lambda$. It is clear that the calculated force on both the sphere and the disk takes a sinusoidal dependence on the sample position with a spatial period of $\lambda/2$, which confirms the above expectation. For the sphere that has a finite size, the actual acoustic radiation force is smaller than King's theoretical prediction, whereas for the disk with $\gamma=4$, the actual force is larger than that on the sphere with the same volume. Therefore, King's formula is not accurate for either spheres with finite size or disklike samples.

The calculated shape factor f as a function of sphere radius is plotted in Fig. 3. At the limit of $R_S\rightarrow 0$, f approaches unity, which is the case of King's approximation. When the sample size increases, f decreases gradually. This means that the increase of the sample size will result in a decrease of the acoustic radiation force per unit volume of the sample. Since the gravity exerted on the sphere is proportional to its volume, the enlargement of the spherical sample size has disadvantages for efficient levitation. A comparison between the calculated data and Leung's formula [Eq. (3)] shows a good agreement at small values of R_S. But a distinct difference appears when R_S approaches $\lambda/4$. The decreasing tendency of the calculated data is steeper than Leung's formula.

In order to discuss the disk samples, we define the shape factor f of a disk as the ratio of the actual force to that expressed by Eq. (1). The shape factors for disks with $\gamma=1$ and $\gamma=2$ are also plotted in Fig. 3 for comparison. It is obvious that f is a function of R and γ.

Figure 4 presents the calculated radiation force on different shapes of disks. The data for spheres and King's formula are also plotted as a reference. In King's theory, the size of the spheres will not influence the levitation result, since the acoustic radiation force and the gravity are both proportional to R^3. However, the actual levitation force deviates seriously away from the R^3 law when R increases, no matter whether it is for disks or spheres. Although a large R in the limit of $R/\lambda\rightarrow 0.25$ makes the levitation inefficient, it can be found that in some cases (for instance, the disks with $\gamma=4,8$, and 16), the levitation force per volume is possible to be enhanced to a great extent, which is interesting for experimental work.

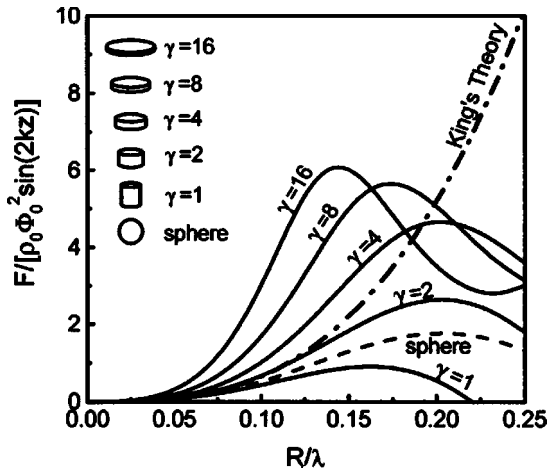

FIG. 4. Dependence of the acoustic radiation force amplitude on the equivalent radius R of disks with different γ values. King's theory gives R^3 dependence.

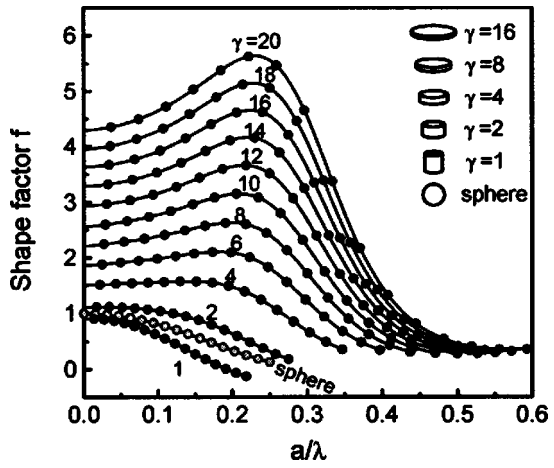

FIG. 5. Dependence of the shape factor f on disk radius a and aspect ratio γ. When γ is larger than a critical value γ^* and a is smaller than a critical value a^*, f increases monotonously rather than decreases with the increase of a.

The shape factor f of disks as a function of disk radius a under different γ values is summarized in Fig. 5. It can be seen that when $\gamma \geqslant 2$, the shape factor of disks is always larger than that of spheres with the same cross-section radius. In addition, there exists a critical value of a^*, at which f attains the maximum value f_M. The trace of $a^*(\gamma)$ can be depicted in a-γ space, as shown in Fig. 6. In order to generate an increasing segment in the f-a curve, it is required that γ should be no less than a critical value of γ^* and a should be no more than a^*. The value of γ^* is estimated to be about 1.9 and a^* would not exceed 0.25λ. Within the range of $a \leqslant a^*(\gamma)$ shown in Fig. 6, the f value for disks increases instead of decreases as for spheres with the increasing of R. The larger the γ value, the larger the f and a^* values are, which indicates that "thin" disks are more efficient than "thick" ones in acoustic levitation. If $a > a^*(\gamma)$, the f-a curves will decrease rapidly, especially for disks with large γ values. This suggests that in practical experiments, the disk

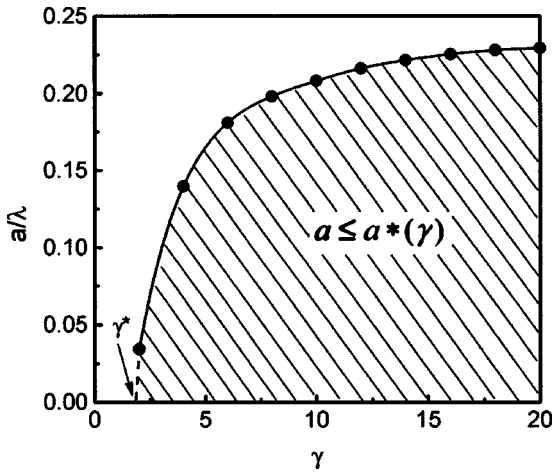

FIG. 6. The critical value a^* as a function of γ. The shadow region represents the condition $a \leqslant a^*$, under which the shape factor f increases monotonously with a. The critical value γ^* is estimated to be about 1.9, and a^* would not exceed $\lambda/4$.

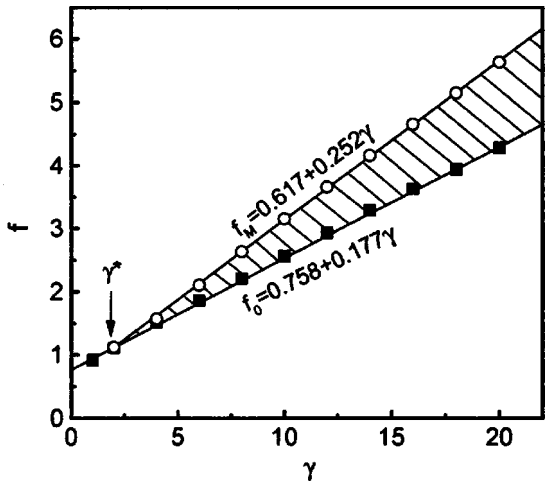

FIG. 7. f_0 and f_M as a function of γ. The shadow area denotes the range of f values ($f_0 \leqslant f \leqslant f_M$) when $\gamma > \gamma^*$ and $a \leqslant a^*$. The open circles and solid squares are simulated data of f_0 and f_M, respectively. The lines are fitted results.

radius should be restricted in an appropriate range in order to get the largest levitation force. Roughly speaking, the disk radius should not exceed 0.25λ.

The value of f at the limit of $a \to 0$, defined as f_0, is also an important quantity, which along with f_M can be used to modify King's formula of Eq. (1) so as to predict the acoustic radiation force on small thin disks. This modified formula is written as

$$F = -\tfrac{5}{6} f(\gamma, R)\, \pi \rho_0 \Phi_0^2 (kR)^3 \sin(2kz), \tag{8}$$

or

$$F = -\frac{5}{4} \frac{f(\gamma, a)}{\gamma}\, \pi \rho_0 \Phi_0^2 (ka)^3 \sin(2kz), \tag{9}$$

in which $f_0(\gamma) \leqslant f(\gamma, a) \leqslant f_M(\gamma)$, $a \leqslant a^*(\gamma)$, and $\gamma > \gamma^*$.

The values of f_0 and f_M as a function of γ are plotted in Fig. 7. Both of them show a good linear relationship,

$$f_0(\gamma) = 0.758 + 0.177\gamma, \tag{10}$$

$$f_M(\gamma) = 0.617 + 0.252\gamma. \tag{11}$$

Under the condition of $\gamma > \gamma^*$ and $a \leqslant a^*(\gamma)$, the values of f in Eqs (8) and (9) are confined to the range $f_0(\gamma) \leqslant f \leqslant f_M(\gamma)$, as shown in the shadow area in Fig. 7.

The acoustic radiation force on an object is the sum of the z component of the radiation pressure normal to the sample surface. Therefore, the levitation force on a disk comes from the contribution of the radiation pressure on the cross sections of this disk. Hasegawa defined a radiation force coefficient Y_{st} for spherical samples [30],

$$Y_{\mathrm{st,sphere}} = \frac{F}{\pi R_S^2 E_A \sin 2kz}, \tag{12}$$

which means the maximum force per unit incident energy density and per unit cross section of the sphere. In Eq. (12), $E_A = \rho_0 k^2 \Phi_0^2 / 2$ is the mean energy density of the incident

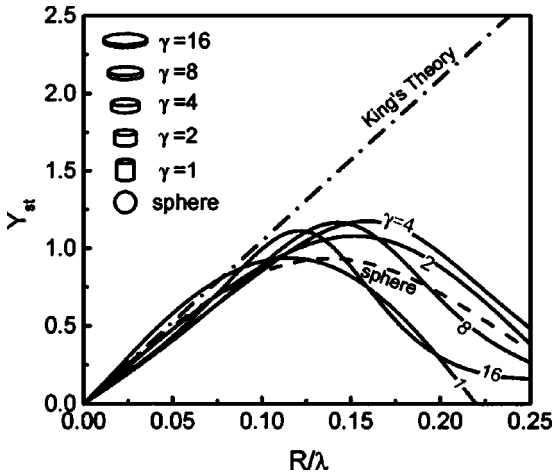

FIG. 8. Dependence of Y_{st} on the equivalent radius R of different disks and spheres. When $R<0.1\lambda$, an approximate linear relationship $Y_{st}=\frac{10}{3}\pi R/\lambda$ can be obtained no matter what shape the sample takes.

planar standing wave. In order to discuss the situation of disks, we modify Eq. (12) by replacing the sphere radius R_S with the disk radius a,

$$Y_{\mathrm{st,disk}} = \frac{F}{\pi a^2 E_A \sin 2kz}, \tag{13}$$

which can be applied to analyze the radiation force coefficient of disk samples.

Figure 8 shows the dependence of Y_{st} on the equivalent radius R of disks and spheres. According to King's formula, Y_{st} is linearly dependent on R, i.e., $Y_{st}=(10/3)\pi R/\lambda$, indicating that the mean acoustic radiation force on the unit cross section of a sample is proportional to its equivalent radius. This is approximately true for all the calculated data of spheres and disks when $R<0.1\lambda$, as shown in Fig. 8. In other words, under the condition of $R<0.1\lambda$, the acoustic radiation force coefficient Y_{st} shows approximately the same linear relationship to the equivalent radius R of the sample no matter what shape the sample takes. According to Eq. (13), F is proportional to the sample cross section. Since a "thin" disk has a larger cross section than a "thick" disk or a sphere with the same volume, the total force on the former is larger than the latter.

III. DYNAMICS OF ACOUSTICALLY LEVITATED WATER DROPS

A. Experimental investigation

The levitation experiment is performed with a single-axis acoustic levitator, which consists of a magnetostrictive transducer and a reflector with a concave reflecting surface. The frequency of the transducer is 16.7 kHz, which produces a wavelength of 20.36 mm in air. Water drops are injected by a syringe into the levitation position that is near the sound pressure nodal. The acoustic field is kept resonant during the levitation process by careful adjustment of the reflector-emitter interval. With this adjustment, the intensity of the acoustic field can also be changed intentionally to a small extent by strengthening or weakening the resonance.

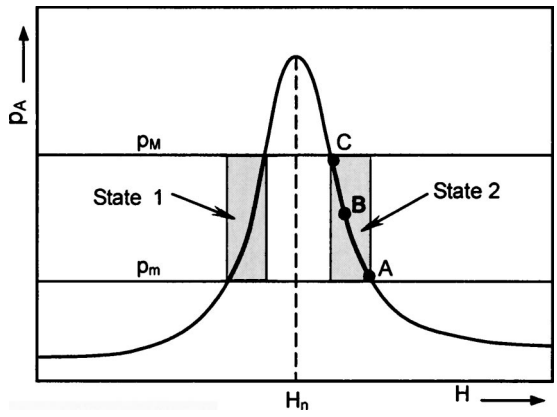

FIG. 9. Schematic of the two possible states of the acoustic field that can levitate a water drop. p_m is the minimum entrapping sound pressure and p_M is the critical atomization pressure. Large water drops (diameter up to 3–4 mm) can only be levitated in state 2.

When a drop is acoustically levitated, the sound pressure amplitude of the acoustic field, p_A, must satisfy the condition $p_m \leqslant p_A \leqslant p_M$, where p_m is the minimum pressure to levitate the drop and p_M is the maximum pressure to ensure the drop stability. Under the approximations of a plane standing wave field and a small rigid sphere sample, these two threshold pressures can be expressed as [31]

$$p_m = (1.6\rho_L \rho_0 g c^2 k^{-1})^{1/2}, \tag{14}$$

$$p_M = (3.4\sigma\rho_0 c^2 R^{-1})^{1/2}, \tag{15}$$

where ρ_L is the density of the drop, ρ_0 is the density of the medium, g is the gravitational acceleration, c is the sound speed in the medium, k is the wave number, σ is the surface tension of the drop, and R is the drop radius. If the sound pressure of the acoustic field is less than p_m, the drop will fall down owing to insufficient levitation force. On the other hand, if the sound pressure is larger than p_M, atomization may occur to the drop [25]. In the present experimental case, the actual acoustic field is not a plane standing wave, thus two wavelength-dependent factors $\alpha(\lambda)$ and $\beta(\lambda)$ should be multiplied to Eqs (1) and (2), respectively [31]. In addition, if the drop has a finite size and deforms into a disklike shape, the shape factor defined in Sec. II should also be considered.

Acoustic levitation is generally conducted near the resonant states of the acoustic field, in which the reflector-emitter interval H should be close to the resonant interval H_n to a certain extent [31]. Figure 9 describes two possible states that can satisfy the above condition of $p_m \leqslant p_A \leqslant p_M$ during the adjustment of resonance. The first one is the state that the reflector-emitter interval H is slightly less than the resonant interval H_n (referred to as state 1). And the second is that the reflector-emitter interval H is slightly larger than the resonant interval H_n (referred to as state 2). Nevertheless, the experiment shows that the first state results in the atomization of large water drops, and only a small water drop (whose diam-

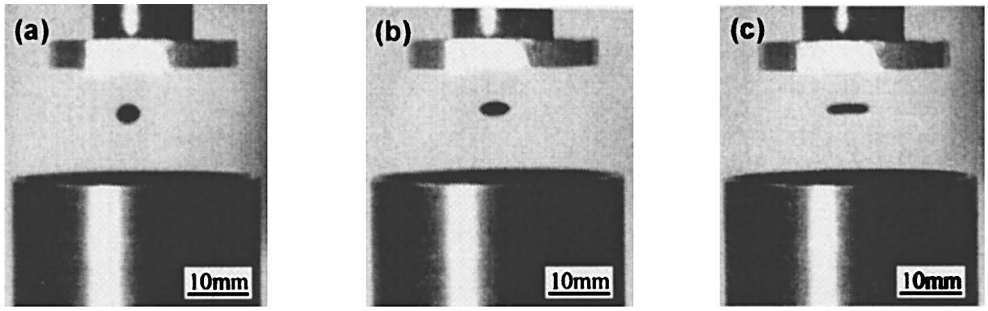

FIG. 10. Deformation of an acoustically levitated water drop with an increase of sound pressure. (a) SPL ~161 dB, (b) SPL ~163 dB, and (c) SPL ~165 dB. The equivalent radius of the drop is about 2 mm.

eter is generally less than 1 mm) can be stably levitated. On the contrary, in the second state, water drops with diameters up to 3–4 mm can be stably levitated.

The acoustic radiation pressure is generally nonuniformly distributed on the drop surface during acoustic levitation, which usually exhibits pressure on the polar area and suction on the equator. This nonuniform radiation pressure leads to the compression in the polar direction and ultimately an oblate shape of the drop forms. The degree of deformation depends on the intensity of the acoustic field. Figure 10 shows the shape development of a water drop levitated in the second state when the reflector-emitter interval is gradually reduced, in which Figs. 10(a), 10(b), and 10(c) correspond roughly to the states marked by A, B, and C in Fig. 9. In Fig. 10(a), where the shape of the water drop is close to a sphere, the drop is likely to fall down because the levitation force in such a state is quite weak. As the sound pressure increases, the water drop deforms into an oblate shape, as shown in Fig. 10(b). When the sound pressure increases further, the drop becomes flatter and the central part of the upper and bottom surface becomes concave, forming a pancakelike shape, as shown in Fig. 10(c). In the state of Fig. 10(c), the acoustic field is the most intense and atomization is likely to occur. Therefore, the state shown in Fig. 10(b) is the most stable one among the above three states. According to the condition $p_m \leqslant p_A \leqslant p_M$, the sound pressure levels corresponding to Figs. 10(a), 10(b), and 10(c) are estimated to be 161, 163, and 165 dB, respectively.

In addition to its deformation, the acoustically levitated drop vibrates translationally in both the vertical and horizontal directions, and oscillates with respect to its centroid as well. The translational vibration is characterized by the to-and-fro movement of the drop centroid with respect to the sound pressure nodal, whereas the shape oscillation is characterized by the alternating expansion and contraction of the drop equator and poles with respect to its centroid. These two kinds of movement are confined by the acoustic radiation pressure and the surface tension, respectively, which will be studied through numerical simulation in the following sections.

B. Formulation of acoustically levitated water drop

When a liquid drop with an originally spherical shape is introduced into an acoustic field, it scatters the incident wave and experiences the acoustic radiation pressure. The distribution of the acoustic radiation pressure on the drop surface is generally nonuniform, which leads to the deformation of this drop under the constraint of the surface tension. The deformed shape in turn modifies the scattered acoustic field and thus the acoustic radiation force on the drop surface. This process repeats and forms shape oscillation and translational vibration of the drop until all the transient energy is dissipated and the final equilibrium shape is reached.

Applying the analysis strategy of Refs. [18,19], and assuming the liquid inside the drop is inviscid and incompressible, the flow is then irrotational and the fluid velocity $\mathbf{u}$ can be expressed as the gradient of the potential Φ_L as $\mathbf{u}=-\nabla\Phi_L$, which satisfies Laplace's equation in the liquid,

$$\nabla^2\Phi_L = 0. \tag{16}$$

The kinematic boundary condition on the drop surface is

$$d\mathbf{r}/dt = \mathbf{u}, \tag{17}$$

where $\mathbf{r}$ is the position of a fluid particle on the drop surface, t is time, and $d/dt=\partial/\partial t+\mathbf{u}\cdot\nabla$ denotes the material differentiation following a given particle. The dynamic boundary condition on the drop surface can be determined from the Bernoulli equation,

$$\rho_L \partial\Phi_L/\partial t + (1/2)\rho_L \mathbf{u}\cdot\mathbf{u} + \Delta P = 0, \tag{18}$$

where ΔP is the pressure difference across the surface which drives the shape oscillation. ΔP is balanced on the surface by

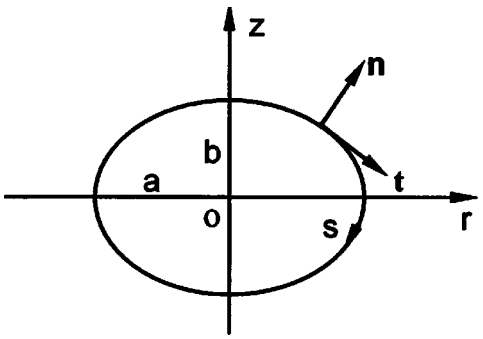

FIG. 11. Coordinate system and description of a water drop. The equatorial and polar radius of the drop are denoted by a and b, respectively.

the surface tension stress, the acoustic radiation pressure P_a, and the gravitational pressure,

$$\Delta P = \sigma \nabla \cdot \mathbf{n} + \rho_L(1-\varepsilon)g(z-z_0) + P_a, \tag{19}$$

where $\mathbf{n}$ is the unit normal vector, $\varepsilon = \rho_0/\rho_L$ is the ratio of air density to liquid density, z is the vertical coordinate, and z_0 is the maximum of z on the drop surface.

Since the period of drop oscillation is much longer than that of the acoustic field, the acoustic radiation pressure exerted on the drop surface is actually the time-averaged value as described by Eq. (6).

For simplicity of calculations, we consider the axisymmetric drop deformation and employ cylindrical coordinates as shown in Fig. 11, where s is the arclength of the generatrix along the drop surface, and a and b are the equatorial and polar radius of the deformed drop, respectively. The characteristic length is defined as the equivalent radius R of the drop in spherical shape, the characteristic pressure $P_0 = 2\sigma/R$ as the surface tension pressure of a spherical drop with radius R, and the characteristic velocity potential as the amplitude of the incident acoustic field, Φ_0. The dimensionless equations describing the evolution of the drop surface can be written as follows:

$$2d\Phi_L/dt = u_t^2 + u_n^2 - \nabla \cdot \mathbf{n} - 2B_0(z-z_0) - W_e\langle \Phi^2 - (\partial\Phi/\partial s)^2/K^2\rangle, \tag{20}$$

$$dr/dt = u_t dr/ds - u_n dz/ds, \tag{21}$$

$$dz/dt = u_t dz/ds + u_n dr/ds, \tag{22}$$

where $B_0 = \rho_L g R^2(1-\varepsilon)/(2\sigma)$ is the gravitational Bond number, $W_e = \rho_0 R k^2 \Phi_0^2/(2\sigma)$ is the acoustic Weber number, $K = kR$ is the dimensionless wave number, and u_t and u_n denote the tangential and normal parts of $\mathbf{u}$, respectively. In Eqs. (20)–(22), the characteristic time, velocity, and fluid velocity potential are $t_0 = (\rho_L R^3/2\sigma)^{1/2}$, $u_0 = (2\sigma/\rho_L R)^{1/2}$, and $\Phi_{L0} = (2\sigma R/\rho_L)^{1/2}$, respectively. By integrating Eq. (20) with respect to time, we can obtain Φ_L and then u_t ($u_t = -\partial\Phi_L/\partial s$). The acoustic velocity potential Φ satisfies the Helmholtz equation and can be solved by the boundary element method described by Eq. (5). Since in this analysis the origin is chosen at the drop centroid, the incident potential is written as $\Phi_{\text{in}} = \sin[K(z-h)]\exp(-j\omega t)$, where h is the distance from the drop centroid to the pressure nodal of the acoustic field. The value of normal liquid velocity u_n can be obtained by solving the Laplace equation (16), which can also be transformed into the boundary integral equation over the drop surface that is analogous to Eq. (5), and solved by the boundary element method. This boundary integral equation is

$$\Phi_L(\mathbf{r}) = 2\int\int \Phi_L(\mathbf{r}')\partial G_L(\mathbf{r},\mathbf{r}')/\partial n dS' - 2\int\int u_n(\mathbf{r}')G_L(\mathbf{r},\mathbf{r}')dS' \tag{23}$$

and the corresponding free-space Green function is $G_L(\mathbf{r},\mathbf{r}') = (4\pi|\mathbf{r}-\mathbf{r}'|)^{-1}$.

TABLE I. Physical parameters used for calculations.

Drop radius	R	2 mm
Frequency	f	16.7 kHz
Sound speed	c_0	340 m/s
Surface tension	σ	0.072 N/m
Gravitational acceleration	g	9.8 m/s^2
Density of water	ρ_L	10^3 kg/m^3
Density of air	ρ_0	1.21 kg/m^3
Characteristic time	t_0	7.454×10^{-3} s

C. Deformation and oscillation of acoustically levitated water drop

Equations (20)–(22) are first-order differential equations which describe the motion of the drop surface with respect to time and can be numerically solved by using the fourth-order Runge-Kutta method. At each step of the iteration, the values of r, z, Φ, u_t, and u_n should be given in advance. The values of r and z can be obtained directly from the previous iteration step, and u_t indirectly by making partial differentiation to the previously obtained Φ_L, whereas the values of Φ and u_n at each step have to be achieved by solving Eqs (5) and (23) by the boundary element method, respectively. In order to accurately describe the drop surface and the derivative quantities such as dr/ds and dz/ds, the cubic b-spline interpolating function is applied. Here, we use eight elements (nine nodes) with equal arclength along the generatrix of the drop surface. And based on the values of Φ at these nine nodes, the values of Φ and $\partial\Phi/\partial s$ between every two adjacent nodes are interpolated by employing the cubic b-spline function. This also enables us to numerically calculate the surface tension pressure $\nabla\cdot\mathbf{n}/2$ and the gravitational pressure $B_0(z-z_0)$.

The initial conditions are set to a spherical water drop with a typical radius $R=2$ mm and zero surface velocity. The incident sound pressure varies from 160 to 166 dB. For a given sound pressure, Eqs. (20)–(22) are numerically solved by using the fourth-order Runge-Kutta method, and the drop shape and surface velocity are recorded with the passage of time. To obtain the equilibrium shape of a levitated drop, the shape oscillation is damped out numerically. When both the ratio of the maximum oscillation amplitude to drop radius and the maximum pressure difference on the drop surface are less than 0.1%, the equilibrium shape is considered to be reached and the computation loops are stopped. In order to speed up the computation process, we also take the equilibrium shape under a certain sound pressure as the initial shape configuration under another sound pressure in practice. For example, the equilibrium shape under 163 dB can be set as the initial shape to be evolved under 162 or 164 dB.

Two gravity conditions are considered. In the zero-gravity ($0g$) case, which corresponds to the microgravity environment in outer space, the drop centroid is located at the sound pressure node of an incident acoustic wave. In the normal gravity ($1g$) case, which corresponds to the terrestrial condition, the equilibrium position of the drop centroid (whose vertical coordinate is denoted by z_c) has to be found before

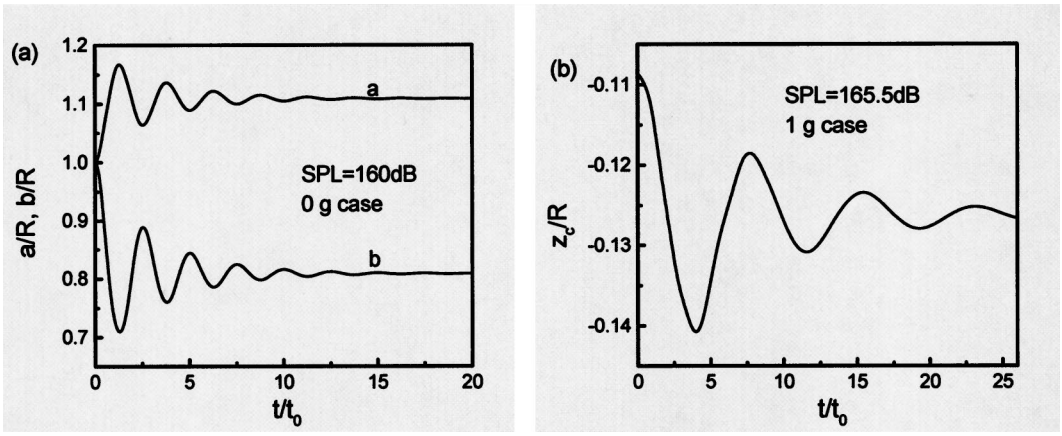

FIG. 12. Temporal evolution of an acoustically levitated water drop. (a) Equatorial radius and polar radius vs time; and (b) centroid position vs time.

the shape evolution begins. This is accomplished by adjusting the parameter of h (the distance from the drop centroid to the sound pressure node) until the resulting force on the drop (assumed to be rigid) is less than a scheduled small value. The parameters and their values used in this simulation are listed in Table I.

Figure 12 shows the temporal evolution of the equatorial radius a and polar radius b of the levitated water drop in acoustic field. z_c is the vertical position of the drop centroid with reference to the nodal plane of an incident standing wave. In order to obtain the equilibrium shapes of the drop under different sound pressure levels, a numerical damping is introduced into the simulation procedures of drop evolution, which can also be seen from Fig. 12. The profiles of the final equilibrium drop shapes under different sound pressure levels are shown in Fig. 13, for both the $0g$ and $1g$ cases. A drop in the zero-gravity condition takes a spherical shape if there is no acoustic field. When the acoustic field is exerted, the drop deforms slightly from the sphere into an oblate shape at first. As the sound pressure increases, the drop becomes more flattened, showing a disklike shape. And at higher sound pressures, the central parts of its top and bottom surface even change from a convex shape to a concave shape. Under the normal $1g$ gravity condition, the variation of the drop shape is primarily the same as that under the zero-gravity condition, except that the drop position is lifted with the increase of sound pressure. This agrees well with the experimental results shown in Fig. 10. In the $0g$ condition, the drop centroid is always located in the plane of the sound pressure node. In contrast, it is always below the nodal plane under the $1g$ condition, and with the increase of sound pressure, the vertical position of the drop centroid is lifted toward the sound pressure node. In the $1g$ condition, the resultant acoustic radiation force has to be large enough to counteract the gravitational force. According to Eq. (14), the minimum pressure to entrap a rigid spherical sample is $p_m = 2665.8$ Pa (SPL = 159.5 dB) in the present case. However, the numerical simulation has shown that the drop cannot be levitated even at 160 dB because the small sample condition $kR(=0.617) \ll 1$ cannot be satisfied. The water drop at 160 dB has an aspect ratio of $\gamma = 1.37$, and its shape factor is estimated to be $f = 0.73$ if it is regarded as a thick disk. Con-

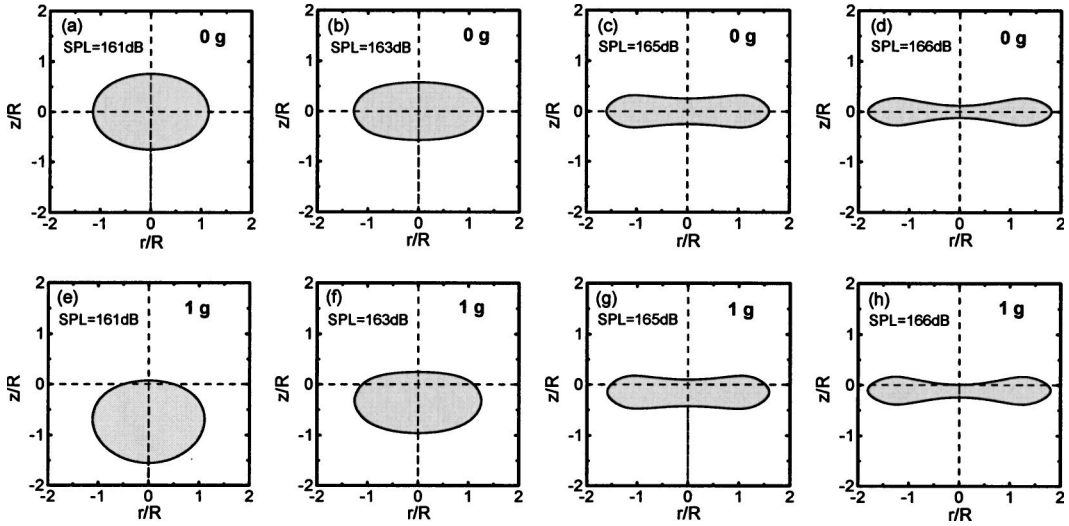

FIG. 13. Equilibrium shapes of an acoustically levitated water drop under different sound pressures. (a)–(d) Zero gravity case: SPL = 161, 163, 165, and 166 dB, respectively; (e)–(h) normal gravity case: SPL = 161, 163, 165, and 166 dB, respectively.

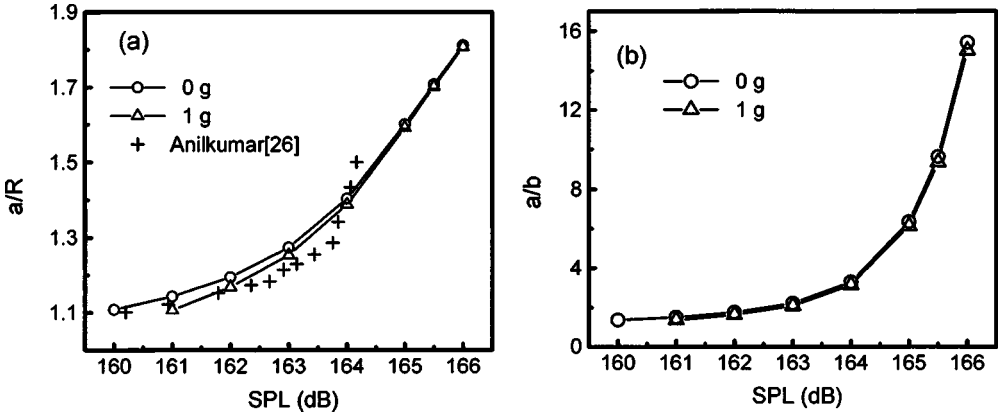

FIG. 14. Deformation of an acoustically levitated water drop. (a) Equatorial radius vs SPL. The crosses are experimental data for a water drop with $kR \approx 0.58$ in Fig. 7 of Ref. [26]. The water drop size in this simulation is $kR = 0.617$. (b) Aspect ratio vs SPL.

sidering the shape factor, the minimum entrapping pressure is recalculated to be 3120 Pa (SPL = 160.8 dB), which is consistent with the simulation.

The deformation of a drop can be indicated by its equatorial radius a or the aspect ratio of the equatorial radius a to polar radius b, as shown in Fig. 14. It can be seen that the equatorial radius and the aspect ratio increase quickly when sound pressure increases. The simulated results are also compared with the experimental data of Anilkumar *et al.* [26] for a water drop with a size of $kR \approx 0.58$, which is close to the condition in the present simulation. It can be seen that the simulation agrees well with Anilkumar *et al.*'s experiment when the deformation is small. The influence of the gravity on shape deformation is not evident, especially when the SPL is large, because at higher SPL, the drop position is very close to the sound pressure node and the incident acoustic field around the drop is similar to that in the 0g case.

On the basis of the temporal evolution of drop surface, we can further obtain the frequencies for both the shape oscillation and the bulk vibration in the vertical direction. These are accomplished by applying a fast Fourier transformation (FFT) program to the temporal evolution of the surface parameters and the drop centroid. Figure 15 shows the FFT spectra of the time evolution of the drop equatorial radius under the 1g condition. The main frequency of the shape oscillation under different sound pressures is determined and plotted in Fig. 16. For a nearly spherical inviscid liquid drop, the frequency of small oscillation is expressed by the Rayleigh relationship [27],

$$f_n = \frac{1}{2\pi}\sqrt{\frac{n(n+2)(n-1)\sigma}{\rho_L R^3}}, \tag{24}$$

where n is the resonant mode number. For the lowest mode $n = 2$, the Rayleigh frequency attains 42.7 Hz in the present case, and is of the same order of the simulated results. Since the acoustically levitated drop experiences a large deformation, it is understood that its oscillation frequency has a deviation from the Rayleigh frequency. Figure 15 shows that, when the sound pressure is larger than 165 dB, there appears an obvious second peak, which corresponds to a higher resonant mode of the shape oscillation. This means that the higher oscillation mode becomes outstanding when larger shape deformation takes place. From Fig. 16, we can conclude that the gravitational field does not apparently affect

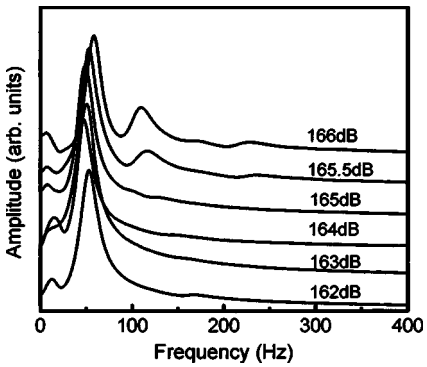

FIG. 15. FFT spectra of the drop equatorial radius oscillation under normal gravity condition with different sound pressure levels. The peak amplitudes define the frequencies of the shape oscillation and bulk vibration in the vertical direction.

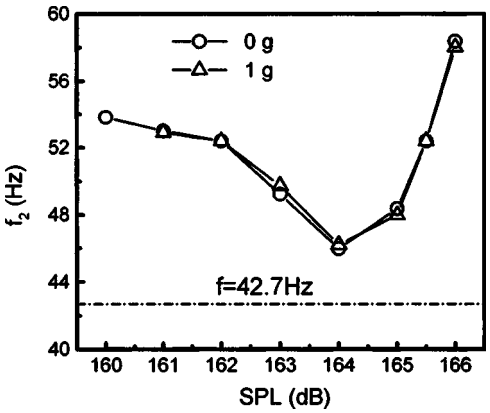

FIG. 16. Oscillational frequency vs SPL for the FFT spectrum shown in Fig. 15. The dot-dashed line represents the oscillational frequency for a spherical water drop predicted by Eq. (24).

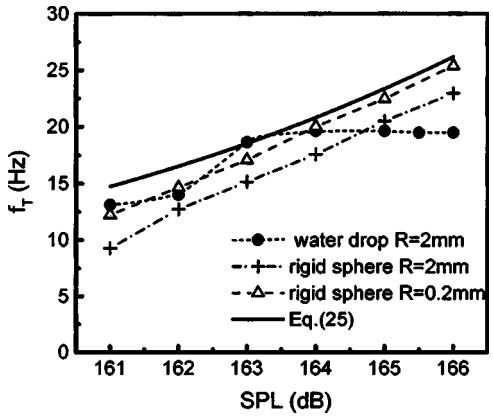

FIG. 17. Translational frequency vs SPL. The solid dots, crosses, and open triangles are simulated data for a water drop (R =2 mm), a large rigid sphere (R=2 mm), and a small rigid sphere (R=0.2 mm), respectively. The solid line is the translational frequency for a small rigid sphere predicted by Eq. (25).

the oscillation frequency, since the shape oscillation is mainly dominated by the surface tension.

The vertical translation frequency is achieved by making a fast Fourier transformation to the time evolution of the drop centroid, and is plotted in Fig. 17. The restoring force of the vertical vibration is provided by the acoustic radiation force. Therefore, the translational frequency is dependent on the intensity of the incident acoustic field. For a rigid small sphere, the resultant acoustic radiation force can be expressed as $F=-(5/6)\pi R^3(\omega/\rho_0 c^3)p_0^2\sin(2kz)$, which can be further approximated as $F=-(20\pi^3R^3p_0^2f^2/3\rho_0c^4)z$ near the sound pressure nodal. In the above expression, the term in the brackets can be regarded as the restoring force coefficient. Therefore, the translational frequency near the pressure nodal can be written as

$$f_T=\frac{p_0 f}{2c^2}\sqrt{\frac{5}{\rho_0\rho_L}}, \tag{25}$$

where p_0 is the pressure amplitude of an incident acoustic field. The frequency predicted by Eq. (25) for different sound pressure levels is shown in Fig. 17 as a solid line, which agrees quantitatively with the simulated result. As a comparison, the translational frequences for a small rigid sphere and a large rigid sphere are also plotted. Equation (25) is derived on the basis of the small rigid sphere approximation, whereas the water drop has a substantial radius and a large shape deformation, and the acoustic radiation pressure also contributes to driving the shape oscillation. Therefore, the deviation between the numerical simulation and Eq. (25) is not surprising.

Although the application conditions for Eqs. (24) and (25) are incompletely satisfied in calculating the oscillational and translational frequencies in practice, and there are indeed certain differences between the analytical and simulated data, the results predicted by Eqs (24) and (25) are still valuable as a quantitative reference. Therefore, Eqs. (24) and (25) are applicable to evaluate the oscillational and translational frequencies to a first-order approximation.

IV. CONCLUSIONS

The acoustic levitation force on disklike samples and the dynamics of the acoustically levitated large water drops are investigated. The acoustic radiation force of a plane standing wave on a disk varies sinusoidally with the sample position, which is similar to the case of a sphere. The dependence of the force amplitude on the equivalent radius R of the disk deviates seriously from the R^3 law predicted by King's formula and a larger force can be obtained for "thin" disks. The shape factor f of spheres and thick disks ($\gamma<\gamma^*$) decreases monotonously with the increase of the sample size, whereas that of thin disks ($\gamma\geqslant\gamma^*$) has an increasing range when the disk radius a is smaller than a critical value a^*. If $a\leqslant a^*$, the acoustic radiation force on a disk in a planar standing wave can be expressed as Eq. (8) or Eq. (9), in which f is mainly a function of γ. The value of $f(\gamma)$ can be estimated by $f_0(\gamma)\leqslant f(\gamma)\leqslant f_M(\gamma)$ where $f_0(\gamma)$ and $f_M(\gamma)$ can be expressed linearly by Eqs (10) and (11). The calculation of the acoustic radiation force coefficient Y_{st} indicates that when $R<0.1\lambda$, the mean acoustic radiation force per unit cross section of a sample is approximately $\frac{10}{3}\pi R/\lambda$, no matter what shape the sample takes. Because thin disks have larger cross sections for the same volume, it is advantageous to obtain a larger acoustic radiation force when levitating thin disks.

The acoustic levitation of a water drop is studied experimentally and a necessary condition of the acoustic field for stable levitation of large water drops is proposed, that is, to adjust the reflector-emitter interval H slightly above the resonant interval H_n. A numerical simulation is conducted to study the deformation and oscillation of a water drop levitated in an acoustic field for both microgravity and normal gravity conditions. It is found that the aspect ratio of the equator radius to the polar radius of the drop increases quickly when sound pressure increases. The original convex shape of the central part of the top and bottom surface even changes into a concave shape at higher sound pressure levels. These results agree well with the experiments. The main frequencies of the shape oscillation under different sound pressures are larger than the Rayleigh frequency because of the large shape deformation. The gravitational field does not apparently affect the oscillational frequencies. The simulated translational frequency is consistent with the analytical result. As a first-order approximation, Eqs. (24) and (25) can be applied to evaluate the oscillational and translational frequencies.

ACKNOWLEDGMENTS

The authors thank Dr. Y. J. Lü for his help with the experimental work. This study was supported by the National Natural Science Foundation of China under Grants No. 50301012, No. 50121101, and No. 50271058, Huo Yingdong Education Foundation under Grant No. 71044, and the Chinese Postdoctoral Science Foundation.

[1] E. H. Brandt, Nature (London) **413**, 474 (2001).
[2] W. J. Xie, C. D. Cao, Y. J. Lü, and B. Wei, Phys. Rev. Lett. **89**, 104304 (2002).
[3] E. H. Brandt, Science **243**, 349 (1989).
[4] W. J. Xie, C. D. Cao, Y. J. Lü, and B. Wei, Phys. Rev. E **66**, 061601 (2002).
[5] A. Biswas, J. Cryst. Growth **147**, 155 (1995).
[6] K. Ohsaka, E. H. Trinh, and M. E. Glicksman, J. Cryst. Growth **106**, 191 (1990).
[7] R. G. Holt and E. H. Trinh, Phys. Rev. Lett. **77**, 1274 (1996).
[8] T. G. Wang, E. H. Trinh, A. P. Croonquist, and D. D. Elleman, Phys. Rev. Lett. **56**, 452 (1986).
[9] S. Santesson *et al.*, Anal. Chem. **72**, 3412 (2000).
[10] S. K. Chung and E. Trinh, J. Cryst. Growth **194**, 384 (1998).
[11] L. V. King, Proc. R. Soc. London, Ser. A **147**, 212 (1934).
[12] L. P. Gor'kov, Sov. Phys. Dokl. **6**, 773 (1962).
[13] M. Barmatz and P. Collas, J. Acoust. Soc. Am. **77**, 928 (1985).
[14] E. Leung, N. Jacobi, and T. Wang, J. Acoust. Soc. Am. **70**, 1762 (1981).
[15] W. A. Oran, L. H. Berge, and H. W. Parker, Rev. Sci. Instrum. **51**, 625 (1980).
[16] P. L. Marston, J. Acoust. Soc. Am. **67**, 15 (1980).
[17] H. W. Jackson, M. Barmatz, and C. Shipley, J. Acoust. Soc. Am. **84**, 1845 (1988).
[18] W. T. Shi and R. E. Apfel, J. Acoust. Soc. Am. **99**, 1977 (1996).
[19] Y. H. Su and Z. C. Feng, J. Acoust. Soc. Am. **99**, 2799 (1996).
[20] E. H. Trinh, A. Zwern, and T. G. Wang, J. Fluid Mech. **115**, 453 (1982).
[21] P. Suryanarayana and Y. Bayazitoglu, Phys. Fluids A **3**, 967 (1991).
[22] X. Zheng, Y. Tian, R. G. Holt, and R. E. Apfel, J. Acoust. Soc. Am. **91**, 2397 (1992).
[23] T. Shi and R. E. Apfel, Phys. Fluids **7**, 1545 (1995).
[24] C. P. Lee, A. V. Anilkumar, and T. G. Wang, Phys. Fluids A **3**, 2497 (1991).
[25] S. D. Danilov and M. A. Mironov, J. Acoust. Soc. Am. **92**, 2747 (1992).
[26] A. V. Anilkumar, C. P. Lee, and T. G. Wang, Phys. Fluids A **5**, 2763 (1993).
[27] E. H. Trinh, P. L. Marston, and J. L. Robey, J. Colloid Interface Sci. **124**, 95 (1988).
[28] Y. Bayazitoglu and G. Hel, J. Thermophys. Heat Transfer **9**, 684 (1995).
[29] Y. Tian, R. G. Holt, and R. E. Apfel, Rev. Sci. Instrum. **66**, 3349 (1995).
[30] T. Hasegawa, J. Acoust. Soc. Am. **65**, 32 (1979).
[31] W. J. Xie and B. Wei, J. Appl. Phys. **93**, 3016 (2003).